Asian Journal of Information Technology 15 (23): 4926-4933, 2016
ISSN: 1682-3915

A Novel Spectral Signature Based Classification Approach for Airborne and Spaceborne Hyperspectral Imagery

S. Chidambaram and A. Sumathi
Department of Electronics and Communication Engineering,
Adhiyamaan College of Engineering (Autonomous), 635109 Hosur, Tamil Nadu, India

Abstract: Hyperspectral images are used in wide range of applications in remote sensing domain such as agriculture, meteorology, mineralogy and surveillance. Hyperspectral images are acquired at vast electromagnetic spectrum of about 400-2500 nm which provide increased sensitivity and high ability to distinguish the objects. Due to its high spectral resolution these images exhibit the spectral signatures unique to specific objects, minerals and vegetation. In this research, we envisages a new spectral signature based classifier in which each pixel is assigned to the exact classes based on the spectral signatures or similar spectral statistical characteristics for the effective classification of hyperspectral images. HyDICE urban image dataset is used to assess the performance characteristics of the proposed algorithm and also compared with conventional classifiers of k-means and fuzzy c-means methods. The experimental results shows that the proposed spectral signature based classification method outperforms the existing classification methods.

Key words: Hyperspectral images, remote sensing, spectral signatures, classification, accuracy assessment

INTRODUCTION

Hyperspectral imagery is becoming emerging trend in remote sensing applications. The present and future space missions are based on the hyperspectral image sensors. Hyperspectral images contain very detailed information of remotely sensed data. Each pixel of the hyperspectral image cube is represented with hundreds of different wavelengths and these contiguous images are formed as three dimensional image cube includes two spatial coordinates and one spectral coordinate.The image cube obtained by the imaging spectrometer of NASA owned Airborne Visible/Infrared Imaging Spectrometer (AVIRIS) includes 224 spectral bands of 512×614 sized pixels (1). Because of its high degree of spectral content, identification and classification of features, patterns and objects in these images are cumbersome. Hyperspectral sensors capture energy in 200 bands or more which means that they continuously cover the reflecting spectrum for each pixel in the scene (Vorovencii, 2009). Bands characteristic for these types of sensors are continuous and narrow, allowing an in-depth examination of features and details on the earth surface. Most hyperspectral sensors are mounted on aerial platforms. In general, the spectral range within which hyperspectral sensors on aircraft work is 380-12700 nm and for those on the satellites is 400-14400 nm. Unlike the sensors on aircraft, sensors on satellites have the capacity to provide global coverage at regular intervals (Vorovencii, 2009). Hyperspectral image cubes are generated from airborne and spaceborne platforms. Many airborne based imaging spectrometer and spaceborne based imaging spectrometer with several number of bands are developed and operational by various countries and research organizations. The main focus of this research is to propose an effective and efficient classification scheme required to distinguish the objects presence in hyperspectral images.

Literature review: Hyperspectral image classification using spectral-spatial constraint proposed by Ji *et al.* (2014) in which the pixels are classified based on the constructed hypergraph includes feature based hyperedge and spatial based hyperedge with the assumptions that the pixels which are close in the feature region or space and the pixels which are spatially closure maximally belong to the same class. Kang *et al.* (2014) incorporated spatial and spectral similarity measures for both dimensionality reduction and hyperspectral image classification based on the observation that the pixels within the close region are spatially related and spectral similarity measures exploits the redundancy for dimension reduction. Wang *et al.* (2015) proposed the Spectral Frequency Spectrum Difference (SFSD) method which

Corresponding Author: S. Chidambaram, Department of Electronics and Communication Engineering,
Adhiyamaan College of Engineering (Autonomous), 635109 Hosur, Tamil Nadu, India

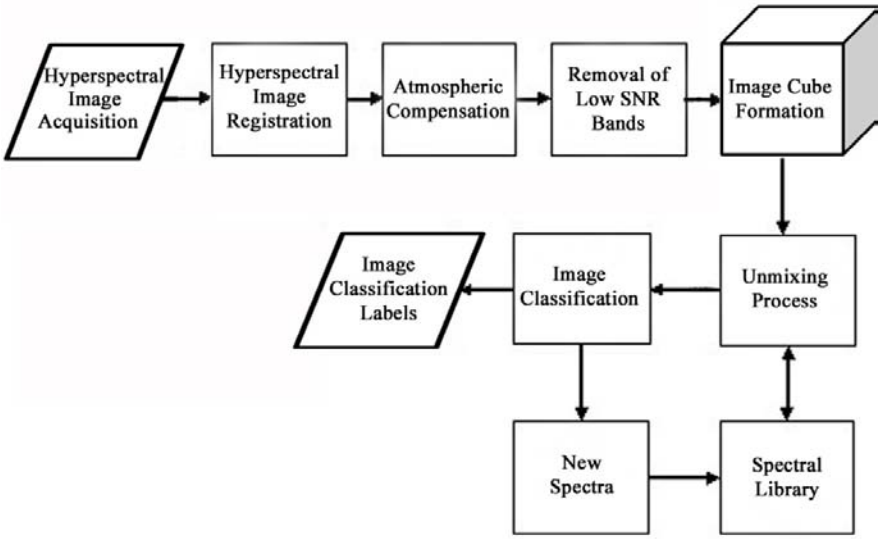

Fig. 1: Proposed system architecture for hyperspectral image classification

determines the spectral similarity in frequency domain using Fourier transform with the concept that the characteristics of spectral signature can be obtained clearly in frequency domain. Erlei developed a sparse representation based classifier with Spectral Information Divergence (SID), exploiting the spectral discrepancy between the two pixels for the effective hyperspectral image classification. Hongzan developed an Unsupervised Spectral Matching based on artificial DNA computing (UADSM) in which dynamic and artificial DNA computing strategy has been incorporated over a spectral signature for effective classification of hyperspectral images. Hyperspectral image classification based on sparsity model (Chen *et al*., 2011) in which sparse representation is used to represent hyperspectral pixels. In this algorithm, two approaches are proposed to improve the performance of classification.Using explicit smoothing constraint, a pixel represented with similar spectral characteristics and mixed pixels are represented by joint sparsity model. Zhang *et al*. (2014) proposed a new spectral-spatial classifier exclusively addresses the problem of mixed pixels. Here, the spectral information can be characterized locally and globally for in-depth analysis for the determination of mixed components in each pixel. Khodadadzadeh *et al*. (2014) proposed edge preserving filtering based approach to improve classification accuracy exclusively for real time applications. Recently, the concept of multiple feature learning for the classification of hyperspectral images proposed by Li *et al*. (2015). This framework is mainly to characterize linear and non-linear features present in the data.

Hyperspectral image classification system: The proposed system framework and its workflow for the classification of hyperspectral image data based on spectral signatures is shown in Fig. 1. The acquisition is performed with a hyperspectral sensor mounted onboard of aerial vehicle. The hyperspectral sensor generally operates in visible region and near Infrared (IR) region provide a rapid and economical technique for finding composition of earth's surface materials of rocks, minerals, soil and water. The image registration is a process of taking multiple satellite or other aerial views of the same surface region and for any given feature of the first view, finding variations if any,that corresponds to it in the second view. Generally this can be done by two approaches viz area based and feature based methods. Atmospheric compensation is required to remove the unwanted components of atmosphere on the computed reflectance values of images. In hyperspectral image analysis, the main goal of algorithms used for atmospheric compensation is to eliminate atmospheric effects such as aerosol scattering, absorption by water vapour and solar illumination effects over the computed spectral information result an accurate estimation of reflectance of the surface. Thus, the obtained surface-reflectance spectra can be compared with the collection of spectral library representing various object (Griffin and Burke, 2003). Hyperspectral sensors mounted on airborne or spaceborne platform acquired these images by computing reflectance data from the surface of earth over a broad range of contiguous wavelengths or spectral bands. Some of the spectral bands are severely affected with low Signal to Noise Ratio (SNR) and do not required for the successive classification of pixels of the hyperspectral image and these bands will be discarded manually by the users before classification. The classification performance significantly improves approximately 10% by the removal

of these unwanted bands while reducing the dimension of the image around 30% in the context of data storage. A general method for displaying hyperspectral imagery is a 3-dimensional image cube. Because of spatial sampling and spectral sampling, Hyperspectral Imaging (HSI) sensors in airborne and spaceborne platform produce a 3-Dimensional (3D) data structure with spatial and spectral components, called as a image cube (Manolakis *et al*., 2003). The high resolution of spectral components in the image allows to discriminate the information at the sub-pixel level with reference to spectral library. In unmixing process, each and every pixel can be modelled as a combination of spectra of various classes referred to as endmembers Carlos Rivera-Borrero. The spectral library which contained endmembers can combined linearly to form all observed spectral signatures. An estimation of the abundance data of the library endmembers for the unknown spectra can be obtained through a vector multiplication matrix of the inverse library matrix and an observed mixed spectra (Singh and Dowerah, 2010). In this context, the attainment of spectral similarity is assessed based on the measure of spectral shape or spectral slope (Christophe *et al*., 2005; Chang, 2013). Unmixing process which is based on sub-pixel level is an effective method in classifying hyperspectral images with its unique spectra.

MATERIALS AND METHODS

The main focus of the proposed scheme is the assignment of each pixel to the correct class based on the similar spectral statistical characteristics. Let $X = \{x_1, x_2, x_3, ... , x_m\}$ be a hyperspectral image dataset with M number of spectral bands. After removing low SNR bands ,it is denoted as $X = \{x_1, x_2, x_3,...., x_n\}$ .Let $X_k = \{x_{1,k}, x_{2,k}, ... , x_{n,k}\}^T$ represents the spectral vector of k^{th} pixel of all the required bands.We note that every pixel is a linear combination of different spectra of N endmembers. Let X_i be the ith pixel of hyperspectral image and its linear spectral mixture is expressed by the following Eq. 1:

$$X_i = \sum_{j=1}^{N} \left(M_{ij} \times S_j\right) + \varepsilon_i \quad (1)$$

Where:

M_{ij} = The spectral reflectance of the jth endmember for the ith band

S_j = The proportion value of the jth endmember

ε_i = The sensor noise or errors in the ith band

Consequently, it is possible to model each pixel of hyperspectral image as a linear combination of a finite set of components as follows:

$$\begin{aligned} X_1 &= M_{11} \times S_1 + M_{12} \times S_2 + ... + M_{1N} \times S_N + \varepsilon_1 \\ X_2 &= M_{21} \times S_1 + M_{22} \times S_2 + ... + M_{2N} \times S_N + \varepsilon_2 \\ X_P &= M_{P1} \times S_1 + M_{P2} \times S_2 + ... + M_{PN} \times S_N + s_N \end{aligned} \quad (2)$$

Consider that $X_i = \{x_1, x_2, ..., x_k\}^T$ is a pixel vector or Pixel of Interest to be classified in a hyperspectral image. Let, $W_i = \{w_1, w_2, ..., w_k\}^T$ represents the values of the randomly selected reflectance spectra of well updated spectral library.The classification of a pixel can be formed according to the expression in Equation:

$$X_i W_i; \; i = 1,....k \quad (3)$$

The vector X_i is a spectral content values for the pixel. These values will be tested against the random spectra of spectral library for its high degree of correlation based on the Threshold value (T) where T is chosen as the average of reflectance values. If correlatively equals or exceeds T, the pixels are classified with a label corresponding to matched spectra otherwise another spectral signature will be selected for correlation activity. The summary of the whole classification process is illustrated in Algorithm 1.

Algorithm 1 Spectral Signature Based Classification

Input: The Hyperspectral Image Dataset with relevant bands $X = \{x_1, x_2, x_3, ..., x_n\}$

Output: The Classified Image with color labels indicates different classes

Step 1: Construction of Spectral Signature
For every pixel
{
Compute reflectance values of the Pixel of Interest(PoI) for N bands
Formulate the spectral signature of the Pixel of Interest $X_i = \{x_1, x_2 , ... , x_k\}^T$
Test X_i with standard spectral library for its correlation based on the spectral similarities with threshold values(T).
}
Step 2: Existence of Similarity
if $X_i W_i$ for i = 1, ...k then
classification of the pixels with a label corresponding to matched spectra
else
choose another spectra and repeat the process until X_i meet the requirement
end if

Hyperspectral image dataset: The classification results simulated below are based on the analysis of hyperspectral dataset namely urban dataset. The urban dataset was acquired by Hyperspectral Digital Image Collection Experiment (HyDICE), airborne based sensor over Copperas Cove, an urban area in Texas. It contain 210 bands between a range 0.4-2.5 μm spectral region (Yang *et al*., 2012) at nominal spectral resolution of 3 nm. The segment used in experiments corresponds to 307×307 pixel subset of Urban dataset. The poor Signal to Noise Ratio (SNR) bands and bands of water absorption were deleted prior to analysis. After discarding the image bands containing no information; 160 bands are used for classification. The image in RGB color composition is

Fig. 2: HyDICE image in RGB color composition

Fig. 3: Ground truth of HyDICE Image with 10 mutually exclusive classes

shown in Fig. 2. It contains ten main classes such as building A, building B, road A, road B, parking area, concrete white soil, soil, grass and Tree. The corresponding ground truth of HyDICE image (Yan, 2011) is shown in Fig. 3.

This dataset is publically available at http://www.agc.army.mil/hypercube/. Totally, ten points were chosen to represent various manmade and natural materials in the image and it forms the basis for classification of various classes. Figure 4 shows the

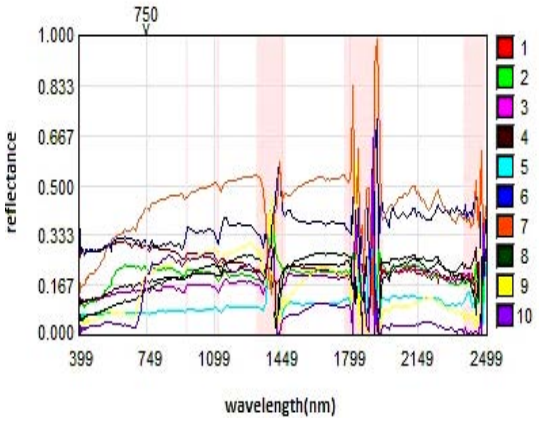

Fig. 4: Spectral Signatures of 10 classes used in the simulation

Fig. 5: Classification accuracy of 10 classes

spectral signatures or reflectance spectra of 10 arbitrarily selected main classes depicted in Fig. 3.

RESULTS AND DISCUSSION

The proposed method is tested using HyDICE image and also compared with the existing classifiers, k-means and fuzzy c-means methods. In order to verify the efficiency of the proposed method, experiments were conducted and the effect of different parameters on the classification accuracy is discussed. As shown previously in Fig. 3, there were 10 classes and each will be classified based on its spectral signatures with a color label during its classification for visual representation of classification results. In this analysis, we used classification accuracy as a primary performance metric. Classification accuracy is the ratio of number of truly classified pixels to the number of total classified pixels.

$$\text{Classification accuracy} = \frac{\text{Number of truly classification pixel}}{\text{Number of available pixel}} \times 100 \quad (4)$$

The results of the comparison of classified images with various classes obtained by the three classifiers using overall accuracy is shown in Table 1. The experimentation shows that the classification accuracy improved significantly with reference to the other traditional methods. When the threshold values are high, the classification is more informative however classification accuracy is compromised. If the threshold values are moderate, the classification accuracy is significantly improved but true classification of pixels cannot be expected. The main focus of our algorithm is

Table 1: Classification results and overall accuracy

	Classification accuracy (%)		
Class	k-means	fuzzy c-means	Proposed
Building A	96.84	97.51	98.91
Building B	97.00	97.91	99.00
Road A	95.96	97.09	98.57
Road B	95.17	96.16	98.02
Parking area	95.59	95.98	97.69
Concrete	97.13	97.93	98.87
White soil	95.87	96.29	98.34
Soil	95.54	96.28	97.88
Grass	92.42	93.85	96.64
Tree	92.85	93.68	96.50
OA (%)	95.44	96.27	98.04

computation of spectral vector and its effective comparison with the spectra of library. The overall accuracy attained by the proposed method is 98.04% which is significantly highest. In HyDICE urban dataset, the proposed method achieves the improvement in overall accuracy of 2.6 and 1.77% with reference to k-means and FCM, respectively. Figure 5 depicts the classification accuracy of the ten different classes obtained by three different classifiers. It is evident that the proposed method gives highest accuracy in all the ten classes. In particular, Building B has classified well among the other available classes. Also proposed method is more effective in the discrimination of Grass and Tree than the traditional classifiers.The classification results for visual comparison obtained by different methods are shown in Fig. 6. The second metric employed to evaluate the goodness of the classification algorithm is precision.It is the ratio of the number of correctly labeled pixels to both correctly and incorrectly classified pixels. These indicators are:

- True Positives (TP): The number of correctly labeled pixels
- True Negatives (TN): The number of correctly labeled pixels belonging to other classes

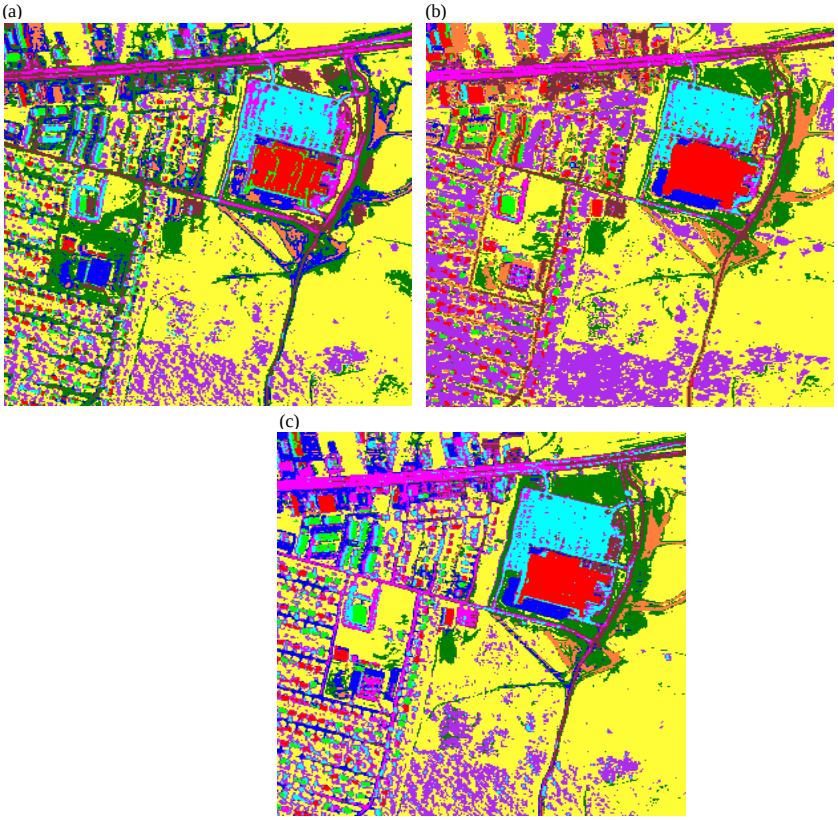

Fig. 6: Classification results by using different methods: a) k-means; b) fuzzy c-means; c) Proposed method

Table 2: Classification results and precision

	Precision		
Class	k-means	fuzzy c-means	Proposed
Building A	75.28	80.32	90.03
Building B	67.78	75.39	86.38
Road A	72.23	79.73	88.19
Road B	65.48	72.34	86.62
Parking area	78.44	79.31	88.44
Concrete	45.87	57.29	72.90
White soil	60.89	65.06	84.24
Soil	67.41	72.09	84.24
Grass	86.63	88.60	93.65
Tree	87.79	90.00	95.34

- False Positives (FP): The number of incorrectly labeled pixels belonging to class
- False Negatives (FN): The number of incorrectly classified pixels belonging to other class

$$\text{Prccision} - \frac{TP}{TP + FP} \tag{5}$$

The precision values of the ten different classes obtained by three different classifiers is given in Table 2. It gives a measure of classifiers exactness. In HyDICE urban dataset the proposed method achieves 87% of exact classification in terms of precision metric. It can be seen that the classification of Tree is more precise among other classes. Figure 7 depicts the precision of the ten classes obtained by three different classifiers. The effect of classification is also assessed by recall. It is the fraction of correctly classified pixels to correctly classified pixels with incorrectly classified pixels.

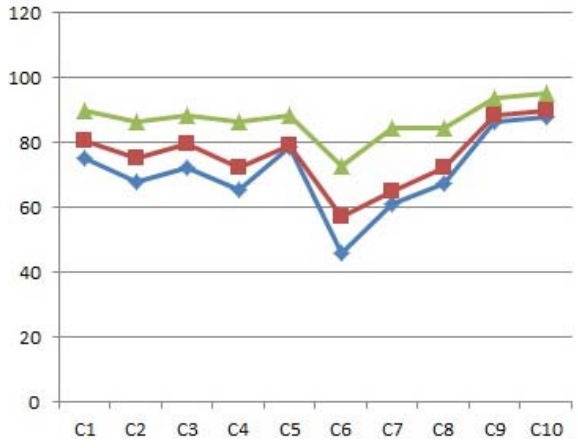

Fig. 7: Precision of 10 classes

Table 3: Classification results and recall

	Recall		
Class	k-means	fuzzy c-means	Proposed
Building A	79.45	83.68	94.43
Building B	81.94	89.49	96.27
Road A	82.78	86.53	95.30
Road B	58.61	68.34	82.08
Parking area	62.96	67.99	81.39
Concrete	65.06	75.86	88.68
White soil	74.84	73.67	85.92
Soil	62.00	70.75	82.67
Grass	79.90	84.58	91.87
Tree	77.88	79.43	87.95

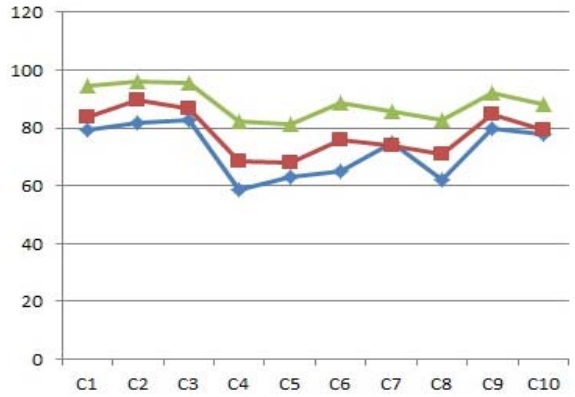

Fig. 8: F-Measure of 10 classes

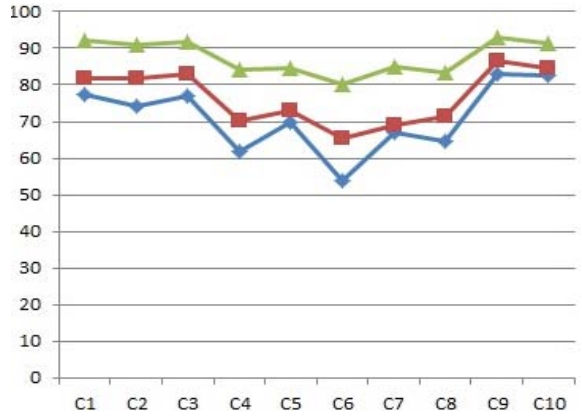

Fig. 9: Classification results by using different methods; a) k-means, b) fuzzy c-means and c) proposed method

$$\text{Recall} = \frac{\text{TP}}{\text{TP} + \text{FN}} \tag{6}$$

Table 3 reports the recall values of the ten different classes obtained by three different classifiers. It gives the classifiers sensitivity. Figure 8 depicts the recall of the ten classes obtained by three different classifiers. A measure that include the harmonic mean of precision and recall is known as F-measure.

Table 4: Classification results and F-Measure

	F-Measure		
Class	k-means	fuzzy c-means	Proposed
Building A	77.31	81.96	92.18
Building B	74.19	81.84	91.06
Road A	77.15	82.99	91.60
Road B	61.86	70.28	84.29
Parking area	69.85	73.21	84.77
Concrete	53.81	65.28	80.02
White soil	67.15	69.10	85.08
Soil	64.59	71.41	83.45
Grass	83.13	86.54	92.75
Tree	82.54	84.39	91.49

$$\text{F} = 2 \times \frac{(\text{Precision} \times \text{Recall})}{(\text{Precision} \times \text{Recall})} \tag{7}$$

Table 4 reports the F-measure of the ten different classes obtained by three different classifiers. This metric maintains the balance between precision and recall. Figure 9 depicts the F-measure of the ten different classes obtained by three different classifiers.

CONCLUSION

In this study, we have presented a novel scheme for the classification of Hyperspectral images. HyDICE urban dataset is used for experimentation. In order to show the effectiveness of classification accuracy, we employed spectral signature based approach as a proposed method in which HSI pixel vector correlated with the spectra of library based on spectral similarities. According to our experimentation, several key findings in terms of overall accuracy, precision, recall and F-measures are reported. The experimental results shows that the classification method using spectral signature based approach improves the overall classification accuracy than the other conventional classifiers.

REFERENCES

Chang, C.I., 2013. Hyperspectral Data Processing: Algorithm Design and Analysis. John Wiley and Sons, New Jersey, USA.,.

Chen, Y., N.M. Nasrabadi and T.D. Tran, 2011. Hyperspectral image classification using dictionary-based sparse representation. IEEE. Transac. Geosci. Remote Sens., 49: 3973-3985.

Christophe, E., D. Leger and C. Mailhes, 2005. Quality criteria benchmark for hyperspectral imagery. IEEE. Transac. Geosci. Remote Sens., 43: 2103-2114.

Griffin, M.K. and H.H.K. Burke, 2003. Compensation of hyperspectral data for atmospheric effects. Lincoln Lab. J., 14: 29-54.

Ji, R., Y. Gao, R. Hong, Q. Liu and D. Tao et al., 2014. Spectral-spatial constraint hyperspectral image classification. IEEE. Trans. Geosci. Remote Sens., 52: 1811-1824.

Kang, X., S. Li and J.A. Benediktsson, 2014. Spectral-spatial hyperspectral image classification with edge-preserving filtering. IEEE. Transac. Geosci. Remote Sens., 52: 2666-2677.

Khodadadzadeh, M., L. Jun, A. Plaza, H. Ghassemian and D.J.M. Bioucas et al., 2014. Spectral-spatial classification of hyperspectral data using local and global probabilities for mixed pixel characterization. IEEE. Transac. Geosci. Remote Sens., 52: 6298-6314.

Li, J., X. Huang, P. Gamba, J.M.B. Dias and L. Zhang *et al*., 2015. Multiple feature learning for hyperspectral image classification. IEEE. Transac. Geosci. Remote Sens., 53: 1592-1606.

Manolakis, D., D. Marden and G.A. Shaw, 2003. Hyperspectral image processing for automatic target detection applications. Lincoln Lab. J., 14: 79-116.

Singh, B. and J. Dowerah, 2010. Hyperspectral imaging: New generation remote sensing. Open Access E. J. Earth Sci. India, 3: 1-14.

Vorovencii, I., 2009. The hyperspectral sensors used in satellite and aerial remote sensing. Bull. Transilvania Univ. Brasov, 2: 51-56.

Wang, K., B. Yong, X. Gu, P. Xiao and X. Zhang, 2015. Spectral similarity measure using frequency spectrum for hyperspectral image classification. IEEE. Geosci. Remote Sens. Lett., 12: 130-134.

Yan, L.M.S., 2011. Region based geometric active contour for classification using hyperspectral remote sensing images. Ph.D Thesis, Ohio State University, Ohio, USA.

Yang, H., Q. Du and G. Chen, 2012. Particle swarm optimization-based hyperspectral dimensionality reduction for urban land cover classification. IEEE. J. Sel. Top. Appl. Earth Obs. Remote Sens., 5: 544-554.

Zhang, E., X. Zhang, S. Yang and S. Wang, 2014. Improving hyperspectral image classification using spectral information divergence. IEEE. Geosci. Remote Sens. Lett., 11: 249-253.